Data-Driven Condition Monitoring for Mooring Systems of a Multi-Float Wave Energy Converter with Two Configurations

Link to publication record in Manchester Research Explorer

Data-Driven Condition Monitoring for Mooring Systems of a Multi-Float Wave Energy Converter with Two Configurations

L. Zhang & P. Stansby & S. Draycott
School of Engineering, University of Manchester, M13 9PL, UK

ABSTRACT: Monitoring the condition of mooring systems is essential for the safe operation and timely maintenance of the wave energy converter. However, mooring dynamics are nonlinearity related to the wave forcing, and are complicated by its coupling with the wave energy converter. These nonlinear and coupling effects pose challenges in accurately identifying the condition of the mooring. In this study, we introduce a data-driven approach for condition monitoring that uses wavelet filtering and dynamic modeling to address these challenges. Initially, a wavelet filter is applied to separate the low-frequency surge motion, attributed to the nonlinear and coupling effects, from the surge at the wave frequencies. Then a linear ARX model is used to build the dynamic relationship between the filtered surge motion and wave surface elevation for monitoring purposes. The effectiveness of this method is demonstrated through its application to two different mooring system configurations within a multi-float wave energy converter. Comprehensive testing across eleven wave conditions confirms the effectiveness of the proposed method.

1 INTRODUCTION

Offshore renewable energy is increasingly recognised as a key component of global electricity generation in the coming decades (Pecher and Kofoed 2017). The reliability of the mooring systems used in these offshore energy projects is a major concern. High failure rates in mooring systems have been reported (Kvitrud 2014). These failures compromise the structural integrity and operational reliability of offshore energy systems and also lead to substantial financial losses. Therefore, condition monitoring of operational mooring systems is highly desirable to detect early faults and prevent catastrophic failures.

The vast majority of existing work uses simulation models for the purpose of developing and validating different condition monitoring algorithms. The popular simulation tools including OrcaFlex, Ansys and FAST are often used to simulate the mooring system response under healthy and damaged conditions. The direct comparison of the time or frequency responses of motions or forces are investigated for severe failures (such as broken lines) (Chung, Pestana, & Kim 2021). These direct comparison may be limited to the normal and severely faulty conditions. For continuous monitoring the condition of the mooring system, neural networks approaches are popular options (Coraddu, Oneto, Walker, Patryniak, Prothero, & Collu 2024). These neural networks algorithms have powerful capacities in modelling different

type of time-frequency variations and non-linearity under different types and severity of faults. However, most of them often require a large amount of training data for training and validating condition monitoring methods. These data may only be available from simulations. The algorithms developed using simulation data alone may not work well for real systems due to the simplification and approximation in the simulation models. Due to the scarcity of data from real systems, especially in the early stages of deploying offshore renewable energy, there is limited research using experimental data collected from physical systems (Ren, Shi, Venugopal, Zhang, & Li 2024).

In this study, a computationally efficient and cost-effective data-driven approach is proposed for monitoring the mooring condition using a small amount of measured wave and surge motion data. The surge motion mainly includes low frequency and wave frequency parts. Although the surge motion has a typical nonlinear relationship with the wave input, it is demonstrated in the paper the the linear relationship can remain for surge motion in the wave frequency part. The linear relationship can be well approximated by a linear dynamic model using limited experimental data, resulting in low computational loading and small data requirements. Further, unlike most of existing work where only simulation data are used, we evaluate the effectiveness of the proposed method on a real mooring system from a multi-float wave energy converter (WEC) M4 using experimental data

under eleven wave conditions (Draycott, Stansby, & Li 2023).

The paper is structured as follows. Section 2 introduces the proposed method. Section 3 presents experiments and results, followed by brief conclusions drawn in Section 4.

2 THE PROPOSED METHOD

In this paper, a data-driven condition monitoring method is proposed for the mooring system of the wave energy converter M4. It has three steps. First, the surge motion data is separated into low frequency and wave frequency parts. Then the relationship between wave surface elevation and surge motion in the wave frequencies is built via AutoRegressive with eXogenous inputs (ARX) model. Finally, a statistical indicator is employed to quantify the difference between the predicted surge from the ARX model and the actual measured surge, commonly known as the residual. The proposed method is illustrated in Fig. 1.

2.1 *Signal separation*

Wavelet filtering is used to separate the surge motion signal into low frequency and wave frequency components. A common method in wavelet filtering is multiple level decomposition. At each level decomposition, the signal is split using selected high-pass and low-pass filters, labeled as h and l, respectively. These filters are determined by the chosen wavelet mother function. The high-pass and low-pass filters operate through convolutions and are then downsampled by a factor of 2. For the first level of decomposition, the raw surge signal s is split into a detailed part D_1 and an approximation part A_1, which are given as (Mallat 1999)

$$D_1(q) = \sum_n s(n)h(n-2q), \quad q = 1, \ldots, \frac{N}{2} \tag{1}$$

and

$$A_1(q) = \sum_n s(n)l(n-2q), \quad q = 1, \ldots, \frac{N}{2}. \tag{2}$$

where $u(n)$ is the measured raw surge data at sample n, $n = 1, \ldots, N$. D_1 contains the detailed coefficients, and A_1 comprises the approximation coefficients. The approximation component A_1 can then be further decomposed into a new set of detailed and approximation components, D_2 and A_2, respectively, referred to as the level 2 decomposition. This process can continue. At the jth level, the decomposition is described by

$$D_j(q) = \sum_n A_{j-1}(n)h(n-2q) \tag{3}$$

and

$$A_j(q) = \sum_n A_{j-1}(n)l(n-2q). \tag{4}$$

A 3-level wavelet decomposition example is shown in Fig. 2. For a wavelet transform up to J levels, the resulting coefficients are given by

$$[A_J, \ D_J, \ D_{J-1}, \ldots, \ D_1]. \tag{5}$$

where the approximation coefficients A_1 capture the lowest frequency range the approximation coefficients while the rest for detailed coefficients cover the middle and high frequency ranges. Since surge motion is characterised by low frequencies and the wave frequencies (middle to high frequencies), the information for each component is captured within these decomposed results. When selecting an appropriate decomposition level J, it is possible to ensure that A_J covers the low-frequency range. Meanwhile, the remaining detailed components capture the wave frequency components. Therefore, to separate surge at wave frequencies, one would use only the detailed coefficients $[D_1, \ldots, D_J]$, while setting all approximation coefficients A_J to zero. Then we can use reconstruction to get the time series data of surge motion at the wave frequencies. The reconstruction is executed in a backward manner using layer-by-layer approach. At the jth level, the reconstruction is given by

$$A_j(q) = \sum_n A_{j-1}(n)l(q-2n)$$
$$+ \sum_n D_{j-1}(n)h(q-2n). \tag{6}$$

2.2 *ARX modeling*

Since the relationship between surface elevation and surge motion at wave frequencies is predominantly linear, we employ a linear ARX model for the identification of the mooring system. The general formulation of the ARX model is given by (Ljung 1999)

$$y(n) = a_1 y(n-1) + \ldots + a_m y(n-m)$$
$$+ b_1 u(n-1) + \ldots + b_l u(n-l) + \xi(n) \tag{7}$$

where the pair set $\{u(n), y(n)\}$ represents input (wave surface elevation) and output (the surge motion at wave frequencies) at time interval n, $n = 1, \ldots, N$, N being the size of the training data set. l and m represent the largest input and output lags, respectively. $\xi(n)$ denotes the error. This ARX model indicates that past input and output values have an effect on the current output value and can be used jointly to predict the future output.
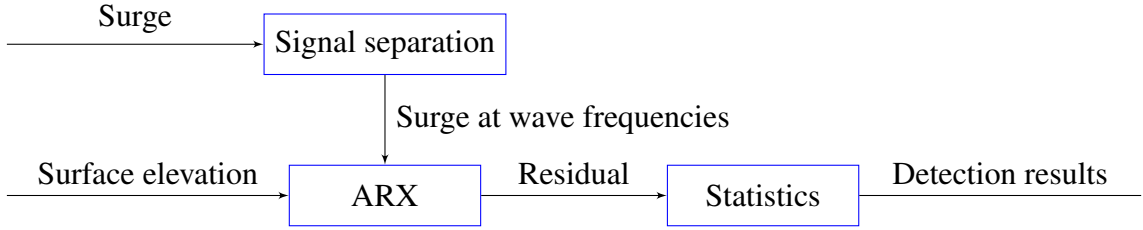
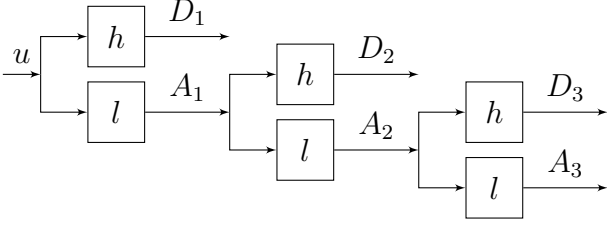Figure 1: The flowchart diagram of the proposed method

Figure 2: Results from a 3-level wavelet decomposition

Since the structure of the ARX model is a linear superposition of a set of input and output variables from the past, it can be formulated as (Ljung 1999)

$$y(n) = \boldsymbol{p}(n)\boldsymbol{\Theta} + \xi(n) \tag{8}$$

where $\boldsymbol{p}(n) = [y(n-1), \ldots, y(n-m), u(n-1), \ldots, u(n-l)]$ is the ARX model regression vector and $\boldsymbol{\Theta} = [a_1, \ldots, a_m, b_1, \ldots, b_l]^T$ is the unknown weighting parameter vector to be optimised. The model (8) can be further rewritten in the matrix form as

$$\boldsymbol{y} = \boldsymbol{P}\boldsymbol{\Theta} + \boldsymbol{\Xi} \tag{9}$$

where $\mathbf{y} = [y(n), y(n+1), \ldots, y(N)]^T$ represents the output vector, $\mathbf{P} = [\mathbf{p}(n), \mathbf{p}(n+1), \ldots, \mathbf{p}(N)]^T$ represents the regression matrix and $\boldsymbol{\Xi} = [\xi(n), \xi(n+1), \ldots, \xi(N)]^T$ is the residual vector. Construction of the ARX models often involves minimising the root mean square error (RMSE).

$$RMSE = \sqrt{\frac{1}{n}\sum_{n=1}^{N}(y(n) - \boldsymbol{p}(n)\boldsymbol{\Theta})^2} \tag{10}$$

using least squares methods. When an ARX model is constructed under healthy conditions, the residuals between the predicted and measured surge motions can be used to differentiate between healthy and damaged conditions. The residual under a healthy condition, denoted as $\boldsymbol{\Xi}_h$, differs from that under a damaged condition, $\boldsymbol{\Xi}_d$. A basic method for evaluation is the calculation of RMSE values. Additionally, in this paper, the statistical Mann-Whitney rank test is employed to distinguish the differences in the distributions of the two sets of residuals (Mann & Whitney 1947).

3 EXPERIMENTS AND RESULTS

In this study, the M4 WEC system is composed of five floats: one bow float, two mid floats, and two stern floats. Two different mooring configurations, named as Configuration 1 and Configuration 2, are used to emulate the normal and abnormal conditions, respectively. Configuration 1 has a 0.2 m diameter hemispherical buoy weighing 1.25 kg, connected to the seabed with three elastic cables and connected to the bow float with one elastic cable, as shown in Fig. 3 and Fig. 4. Configuration 2, as shown in Fig. 5 and Fig. 6, features a smaller buoy, 0.15 m in diameter and weighing 0.21 kg, also connected with three elastic cables. The mooring cable consisted of two latex rubber (exercise) bands in series in the lower part (1.2 m length total) with an inelastic nylon cord to the buoy. The nominal stiffness is 65 N/m with nonlinearity (Draycott, Stansby, & Li 2023). It was found that compared to Configuration 1, the mooring forces of Configuration 2 at the wave frequencies were reduced but the low-frequency forces were not, making them suitable for validating condition monitoring algorithms designed for change detection.
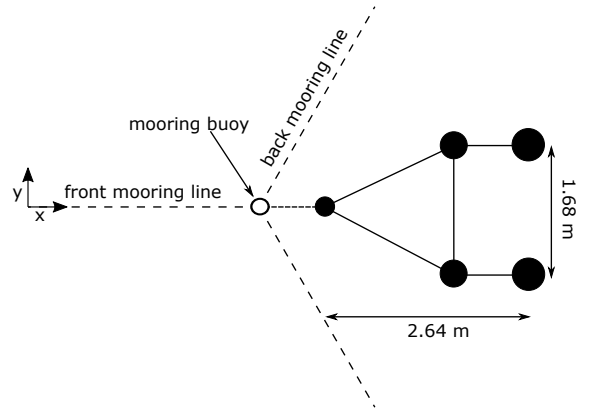

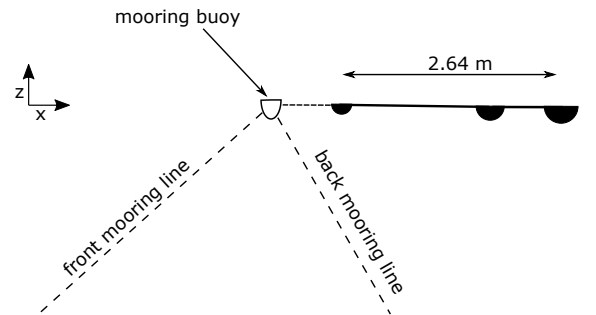Figure 3: Top view of the layout of the M4 WEC and mooring configuration 1

Figure 4: Side-on view of the layout of the M4 WEC and mooring configuration 1

Our experiments were conducted in the ocean basin at the University of Plymouth, UK. Fig. 7 shows the
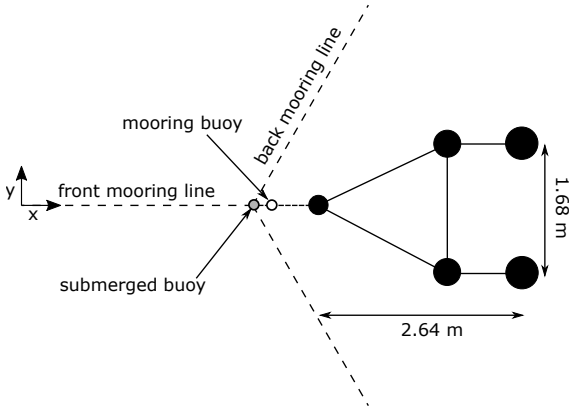
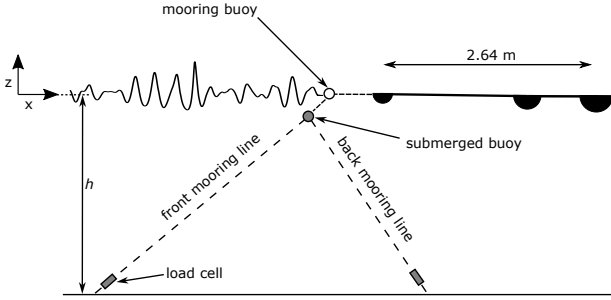Figure 5: Top view of the layout of the M4 WEC and mooring configuration 2

Figure 6: Side-on view of the layout of the M4 WEC and mooring configuration 2. $h = 2$ m is the water depth.

M4 WEC and its mooring system in the wave basin experiment. The experiments were carried out under eleven irregular wave conditions with different wave heights H_s and peak periods T_p. Specifically, four different levels of significant wave heights H_s (0.06 m, 0.09 m, 0.13 m and 0.16 m) and three peak wave periods T_p (1.2, 1.4 and 1.8 s) were considered, and their combinations are detailed in Table 1. The experiments were carried out at a depth of 2 m and each wave condition was tested for a duration of 35 min (2100 s). The 6 DoF M4 motions were recorded using a Qualisys camera system.

Figure 7: A photo of the layout of the M4 WEC and its mooring system in the wave basin

Our previous work demonstrated that pitch motion exhibits a linear relationship with wave surface elevation (Zhang, Draycott, & Stansby 2024). In contrast, surge motion is affected by mooring force and exhibits a nonlinear relationship with wave surface elevation. However, after separating the wave frequency

Table 1: Wave conditions for 11 cases based on JONSWAP spectra. All cases have peak enhancement factor $\gamma = 3.3$.

Case	H_s (m)	T_p (s)	Case	H_s (m)	T_p (s)
1	0.06	1.2	7	0.13	1.2
2	0.06	1.4	8	0.13	1.4
3	0.06	1.8	9	0.13	1.8
4	0.09	1.2	10	0.16	1.4
5	0.09	1.4	11	0.16	1.8
6	0.09	1.8			

surge from the low frequency surge, the relationship with wave surface elevation input becomes predominantly linear. In this study, wave filtering techniques are employed for signal separation. Specifically, the dB4 mother wavelet function and a four-layer wavelet decomposition are used (Mallat 1999). This approach effectively distinguishes the wave frequency surge motion from the low frequency surge across all examined eleven wave conditions. An example of the separation results under case 1 is illustrated in Fig. 8. Panels (a) and (b) display the raw surge motion time series and its spectra, respectively. Panels (c) and (d) depict the low frequency surge and its spectra, respectively, while panels (e) and (f) present the wave frequency surge motion and its spectra, respectively. The results effectively demonstrate that wavelet filtering can successfully differentiate these components due to their distinct frequency ranges.
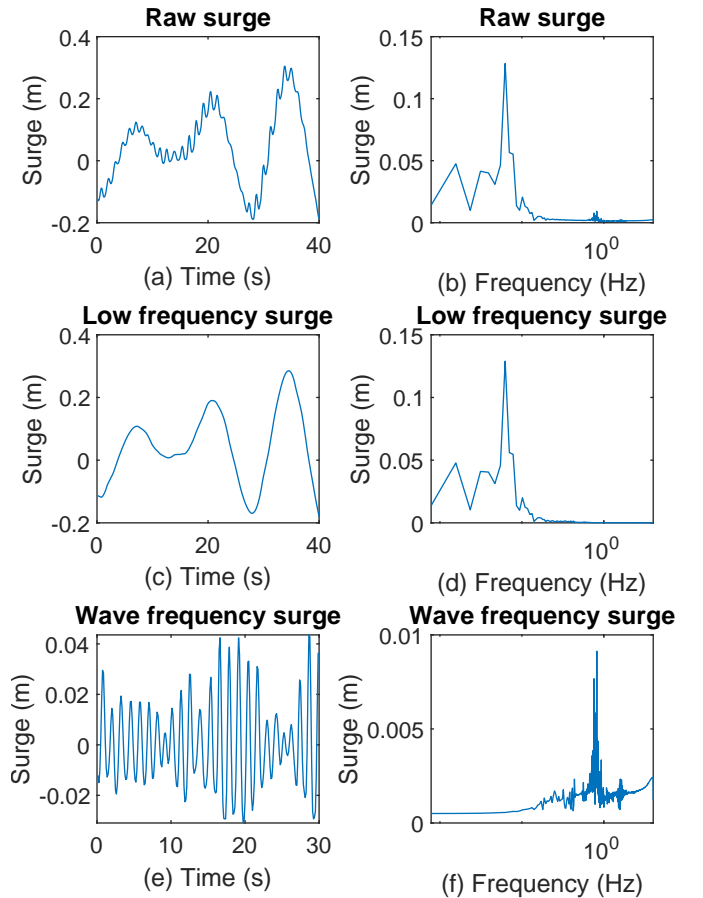

Figure 8: Time series and spectra of raw and separated surge under Case 1 wave condition

The ARX models are trained using the Configu-

ration 1 data under each of the eleven wave conditions, producing eleven ARX models. The input of the training data is the surface elevation and the output of the training data is the surge motion at the wave frequencies. The total amount of the data is 2100 s *8Hz=16800. 70% of the data is used for training and the remaining 30% for validation. Different ARX model orders are compared, and the final model is chosen when both SSE of training and validation is minimised. The modelling process is fast, taking only minutes for all cases. The eleven models are used to predict the surge motion in both Configuration 1 and Configuration 2. The prediction results are shown in Fig. 9 and Fig. 10. It is evident that the results from Configuration 1 are generally better than those from Configuration 2 across all eleven cases. Configuration 1, which is considered a normal and healthy condition, is used for training the models. This training effectively captures the essential dynamics of Configuration 1, resulting in accurate predictions. On the other hand, Configuration 2 simulates an artificial damaged condition as it varies slightly from Configuration 1. The ARX models, originally developed under healthy conditions, are applied to both normal and damaged states. The residuals, namely the differences between the predicted and actual surge motions, can serve as a basis for condition monitoring. Notably, the larger differences in predicted versus measured surge motions under damaged conditions can be used to detect changes in health status.

To further examine the results, the distributions of the residuals between the model predicted surge and measured surge are compared in Fig. 11. Both configurations have bell-curve or normal distributions. Configuration 1 has narrower bell curves while Configuration 2 has flatter bell curves across all the eleven cases although a few cases may have similar distributions (such as Case 6) with Configuration 1. Although the visual differences for these distributions are observed, the manual approach is not preferred in practice. The RMSE results are compared and listed in Table 3. In all the scenarios, Configuration 1 produces smaller RMSE values compared to Configuration 2. Finally, the Mann-Whitney rank test is used to quantify and compare residuals in all eleven cases. When the p-value is below a specified threshold, it suggests a significant difference between two residual distributions. Otherwise, if the p-value exceeds this threshold, there is no statistically significant difference between them. By adopting the widely accepted p-value threshold of 0.05, it is observed that there is one failed detection and the successful detection ratio is 10/11, over 90%, demonstrating the effectiveness of the proposed method. Moreover, this statistical detection process is fully automated, eliminating the need for trial-and-error in setting fault thresholds.
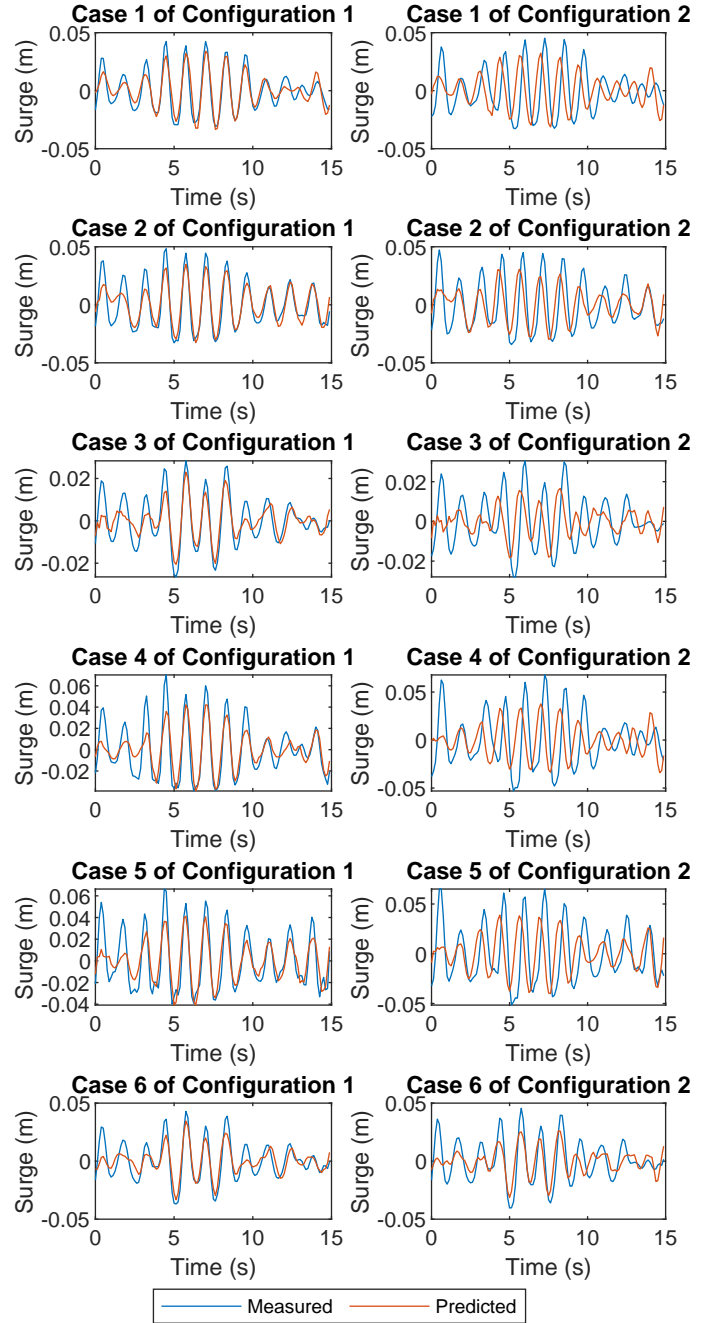

Figure 9: Time series of predicted and measured surge from Configurations 1 and 2 for Cases 1-6

4 CONCLUSION

In this paper, a fast and cost-effective data-driven method is proposed for condition monitoring of mooring systems of a multi-float wave energy converter. First, the proposed method separates the wave frequency component from the total surge motions, allowing for linear relationship analysis under different wave conditions. Then ARX models and statistical results are used to distinguish between normal and altered conditions. The effectiveness of the proposed method has been validated using real experimental data under eleven wave cases. This study has focused on one representative damage condition and future work will explore a range of damage cases.
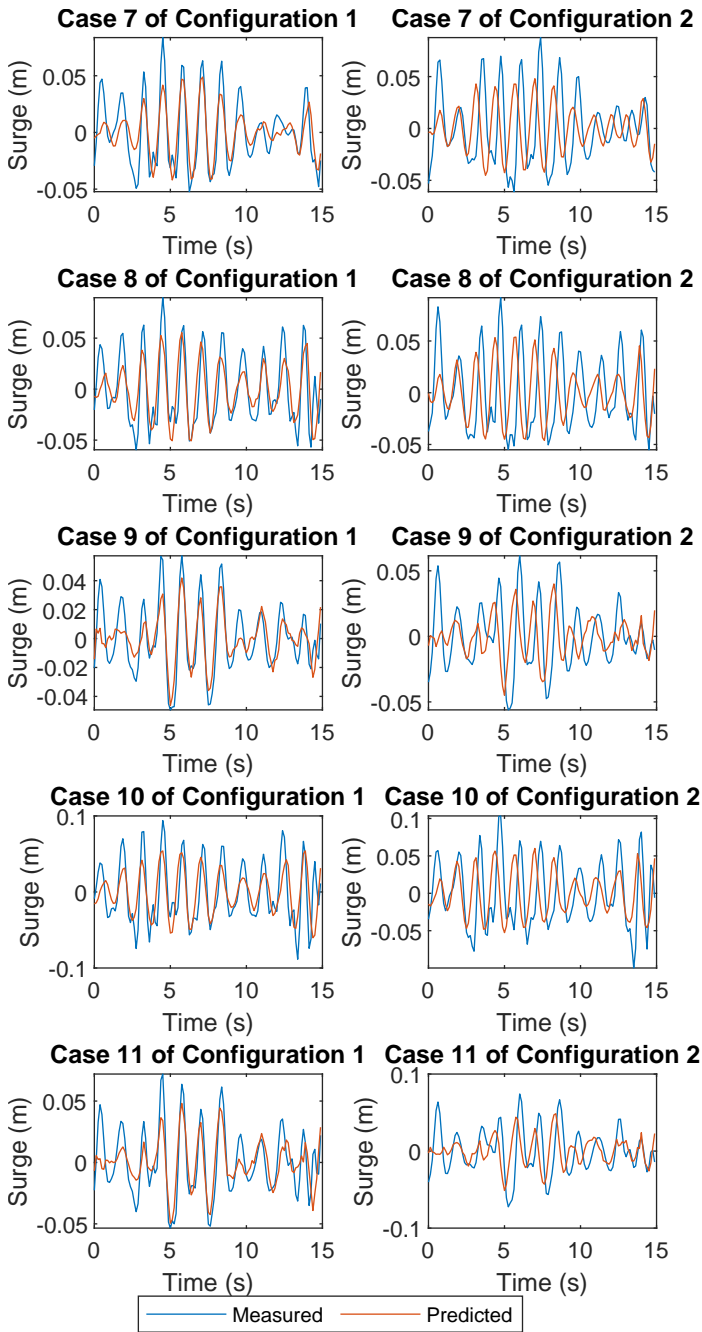
Figure 10: Time series of predicted and measured surge from Configurations 1 and 2 for Cases 7-11

Figure 11: Residual distributions for Configurations 1 and 2

REFERENCES

Chung, W. C., G. R. Pestana, & M. Kim (2021). Structural health monitoring for tlp-fowt (floating offshore wind turbine) tendon using sensors. *Applied Ocean Research 113*, 102740.

Coraddu, A., L. Oneto, J. Walker, K. Patryniak, A. Prothero, & M. Collu (2024). Floating offshore wind turbine mooring line sections health 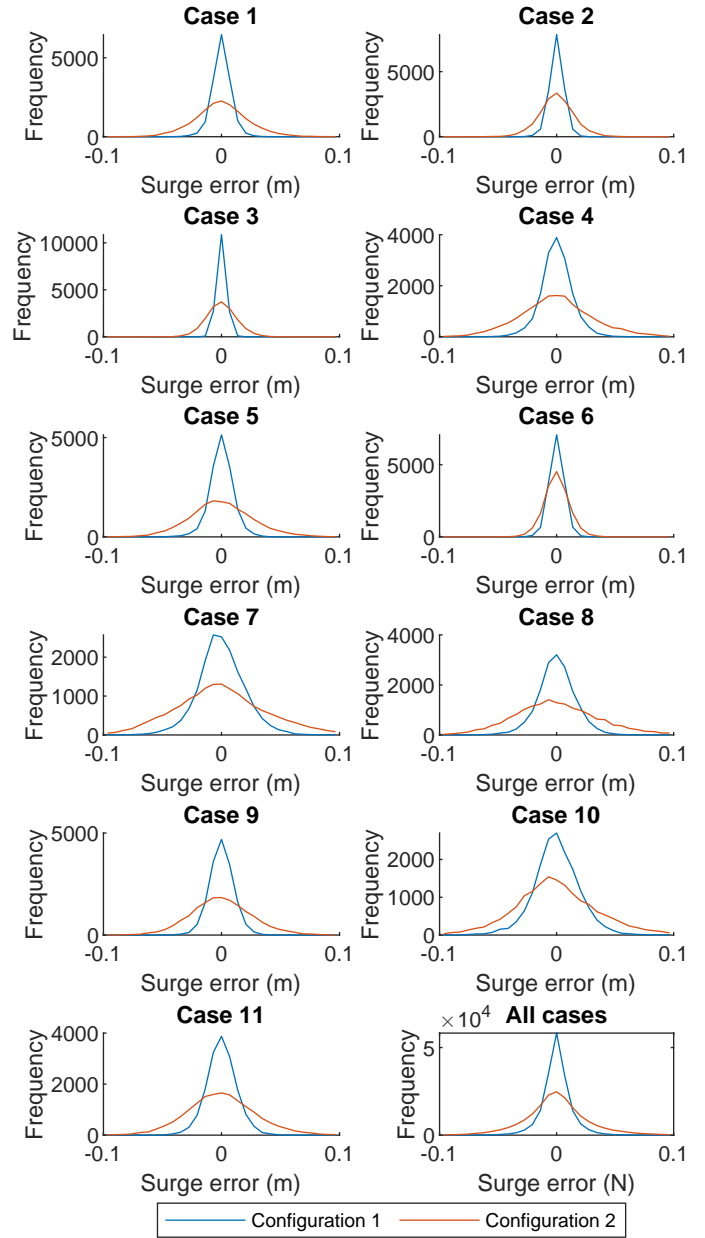status nowcasting: from supervised shallow to weakly supervised deep learning. *Mechanical Systems and Signal Processing 216*, 111446.

Draycott, S., P. Stansby, & G. Li (2023). Experimental measurements of two elastic taut-slack mooring configurations for the multi-float m4 wec. In *European Wave and Tidal Energy Conference, Bilbao, Spain, 3-7 Septemeber*.

Kvitrud, A. (2014). Lessons learned from norwegian mooring line failures 2010–2013. In *International Conference on Offshore Mechanics and Arctic Engineering*. American Society of Mechanical Engineers.

Ljung, L. (1999). *System Identification: Theory for the user* (Second ed.). Prentice Hall.

Mallat, S. (1999). *A wavelet tour of signal processing*. Elsevier.

Mann, H. B. & D. R. Whitney (1947). On a test of whether one of two random variables is stochastically larger than the other. *The annals of mathematical statistics*, 50–60.

Pecher, A. & J. P. Kofoed (2017). *Handbook of ocean wave energy*. Springer Nature.

Ren, Y., W. Shi, V. Venugopal, L. Zhang, & X. Li (2024). Experimental study of tendon failure analysis for a tlp floating offshore wind turbine. *Applied Energy 358*, 122633.

Zhang, L., S. Draycott, & P. Stansby (2024). System identification and generalisation of elastic mooring line forces on a multi-float wave energy converter platform in steep irregu-

Case	RMSE Config 1	RMSE Config 2	Statistics p-value	Statistics Decision
1	0.010	0.023	0.00	Success
2	0.009	0.016	0.00	Success
3	0.008	0.013	0.00	Success
4	0.015	0.032	0.00	Success
5	0.012	0.027	0.00	Success
6	0.009	0.012	0.42	Fail
7	0.021	0.040	0.01	Success
8	0.018	0.037	0.00	Success
9	0.012	0.026	0.00	Success
10	0.021	0.036	0.01	Success
11	0.015	0.030	0.00	Success

lar waves. *Mechanical Systems and Signal Processing 214*, 111259.